



Laser-Driven Transient Phase Oscillations in Individual Spin Crossover Particles

Yaowei Hu, Matthieu Picher, Marlène Palluel, Nathalie Daro, Eric Freysz, Laurentiu Stoleriu, Cristian Enachescu, Guillaume Chastanet, Florian Banhart

► To cite this version:

Yaowei Hu, Matthieu Picher, Marlène Palluel, Nathalie Daro, Eric Freysz, et al.. Laser-Driven Transient Phase Oscillations in Individual Spin Crossover Particles. *Small*, 2023, 19 (39), pp.2303701. 10.1002/sml.202303701 . hal-04109511v2

HAL Id: hal-04109511

<https://hal.science/hal-04109511v2>

Submitted on 30 May 2023

HAL is a multi-disciplinary open access archive for the deposit and dissemination of scientific research documents, whether they are published or not. The documents may come from teaching and research institutions in France or abroad, or from public or private research centers.

L'archive ouverte pluridisciplinaire **HAL**, est destinée au dépôt et à la diffusion de documents scientifiques de niveau recherche, publiés ou non, émanant des établissements d'enseignement et de recherche français ou étrangers, des laboratoires publics ou privés.



Distributed under a Creative Commons Attribution 4.0 International License

Laser-Driven Transient Phase Oscillations in Individual Spin Crossover Particles

Yaowei Hu, Matthieu Picher, Marlène Palluel, Nathalie Daro, Eric Freysz, Laurentiu Stoleriu,* Cristian Enachescu, Guillaume Chastanet, and Florian Banhart*

An unusual expansion dynamics of individual spin crossover nanoparticles is studied by ultrafast transmission electron microscopy. After exposure to nanosecond laser pulses, the particles exhibit considerable length oscillations during and after their expansion. The vibration period of 50–100 ns is of the same order of magnitude as the time that the particles need for a transition from the low-spin to the high-spin state. The observations are explained in Monte Carlo calculations using a model where elastic and thermal coupling between the molecules within a crystalline spin crossover particle govern the phase transition between the two spin states. The experimentally observed length oscillations are in agreement with the calculations, and it is shown that the system undergoes repeated transitions between the two spin states until relaxation in the high-spin state occurs due to energy dissipation. Spin crossover particles are therefore a unique system where a resonant transition between two phases occurs in a phase transformation of first order.

or light. They result in an average local volume increase of $\approx 25\%$ of the coordination polyhedron of the metal site experiencing the spin crossover. In the solid state, the resulting macroscopic volume change can reach up to 10% .^[17] The switchable molecules are linked by weak elastic intermolecular interactions that propagate the local volume change. Depending on the strength of these elastic interactions, cooperative behavior may occur, leading to abrupt, and even hysteretic switching.^[18] Hence, of importance is not only the switching of individual SCO sites but also the interaction between neighboring molecules in different spin states (LS or HS) in a crystal. The propagation of the elastic interaction depends strongly on the size of the system. Hence, while reducing the size of a sample, the cooperativity is generally reduced.^[19]


1. Introduction

Switchable materials belong to the family of smart materials of huge interest in future daily-life applications.^[1] Among them, spin crossover (SCO) materials are highly promising for the realization of switchable devices at the nanoscale with applications as opto-electronic devices,^[2,3] mechanical devices,^[4–9] molecular memories^[10–12] or sensors.^[13–15] The SCO phenomenon is a multiscale process that results from a change of electronic configuration of a coordination complex between low spin (LS) and high spin (HS) states.^[16] The transition starts at the coordination sphere level and propagates through the whole sample. Spin crossover transitions can be induced by temperature, pressure,

The dynamics of the SCO phenomenon have been widely investigated from the femto- to the microsecond timescale on macroscopic and nanoscopic objects using optical pulses as pump and optical or X-ray pulses as probes. The dynamics reveals a multistep process: i) First, the LS to HS photoswitching occurs in a few femtoseconds with a local increase of the coordination sphere volume but at constant unit-cell volume. ii) Second, these newly formed HS molecules generate internal pressure on the LS lattice that induces a pressure wave that propagates at the speed of sound. This results in an increase of the unit-cell volume at the picosecond time scale. iii) Third, the energy deposited by the laser pulse dissipates through lattice heating at a time

Y. Hu, M. Picher, F. Banhart
Institut de Physique et Chimie des Matériaux UMR 7504
Université de Strasbourg & CNRS
Strasbourg 67034, France
E-mail: florian.banhart@ipcms.unistra.fr

M. Palluel, N. Daro, G. Chastanet
Université de Bordeaux
CNRS
Bordeaux INP (ICMCB-UMR 5026)
Pessac 33600, France
E. Freysz
Université de Bordeaux
CNRS UMR 5798
LOMA
Talence cedex 33405, France
L. Stoleriu, C. Enachescu
Faculty of Physics
Alexandru Ioan Cuza University
Iasi 700506, Romania
E-mail: lstoler@stoner.phys.uaic.ro

 The ORCID identification number(s) for the author(s) of this article can be found under <https://doi.org/10.1002/smll.202303701>

© 2023 The Authors. Small published by Wiley-VCH GmbH. This is an open access article under the terms of the Creative Commons Attribution License, which permits use, distribution and reproduction in any medium, provided the original work is properly cited.

DOI: 10.1002/smll.202303701

constant defined by the thermal diffusivity, the density, and the heat capacity of the material. This increase of temperature is faster as the crystal size is reduced.^[20–24]

Due to the switching of individual molecules between the two spin states and pressure or temperature exchange between the molecules, the phase transformation between the LS and HS state is local. However, the global behavior of the crystals, that is, their total volume, results from the propagation of pressure and temperature waves due to the transfer of the spin state between neighboring molecules. Reflection of the waves at the surfaces of the particles may eventually lead to periodic phase changes where the resonance frequency is determined by the size of the particle. In this study, we show that this leads to an oscillating length of the whole crystal with a frequency that is much lower than expected for purely elastic vibration modes. The SCO particles are therefore able to vibrate between the two phases, although the transition between the LS and HS state is a phase transformation of first order. In such first-order transitions, oscillations between two phases do not normally occur due to energy dissipation during the transition. SCO crystals are therefore a unique system to study such resonant phase transformations.

So far, time-resolved studies by optical or X-ray techniques have only given information about large ensembles of SCO (nano)particles, where they might have different sizes or orientations. Therefore, only average information about the behavior of SCO particles was obtained and mainly focused on the elastic wave propagation (fs–ps). As an example, coherent vibrations of a crystal lattice were probed at the 5–20 ps timescale.^[25] Recently, thanks to the development of ultrafast electron microscopes (UTEM), which combine high spatial with high temporal resolution, two studies of SCO particles have been carried out.^[26–28] These investigations have evidenced anisotropic length changes of individual SCO particles after laser pulses at the nanosecond timescale. This technique allows to elucidate the expansion and compression dynamics of individual nanoparticles. Here, we show the appearance of transient oscillations of SCO particles after excitation by optical pulses. This appears to be an important property of SCO nanoparticles that are not accessible to macroscopic measurements due to the averaging over many SCO particles at the same time. We couple this study with Monte Carlo simulations to disentangle the role of elastic and thermal waves in the expansion dynamics of SCO particles. A length oscillation of SCO particles during the switching process is of importance in several applications of SCO materials, especially when contacts with electrodes or fatigue are involved.

2. Results

The 1D coordination polymer $[\text{Fe}(\text{Htrz})_2\text{trz}](\text{BF}_4)$ shows changes in the unit-cell volume by 11% under heating with a pronounced elongation of the *b* axis (axis along which the 1D polymer grows) of 0.46 Å from LS to HS, corresponding to an expansion of 6%.^[28,29] This size change makes it possible to trigger and image the photoswitching process by following the size expansion as a function of time and laser fluence.

Figure 1 shows time-resolved measurements of the expansion of two individual SCO particles at a laser wavelength of 532 nm. The expansion along the *b*-axis of the SCO crystal starts ≈ 10 –20 ns after the laser pulse and then shows a first saturation step

at 3–4% expansion until at 100 ns the expansion reaches its maximum value of 6%. This corresponds to the LS to HS transformation. It is apparent that length instabilities much higher than the measurement error (0.2–0.3%) appear during and after both expansion steps. After ≈ 500 ns, the length stabilizes and only shows slight length variations until the particle shrinks that occurs after some 100 μs . This corresponds to the HS to LS relaxation. The recovery of the LS state after ≈ 1 μs permits a stroboscopic experiment at a repetition rate of 20 Hz.

The appearance of these instabilities was further studied at different wavelengths of the laser pulses and on smaller particles. At higher irradiation wavelengths, a higher intensity of the pulses is needed to reach 6% expansion. This is seen in **Figure 2a,b** where the expansion at 1064 nm occurs smoothly and the vibration is only visible after saturation at 100 ns and with less amplitude than after a 532 nm pulse. This originates from the lower absorption of SCO in the near infrared that decreases the efficiency of the photothermal effect. A smaller particle (390 nm) was irradiated with 1064 nm pulses (**Figure 2c**). It shows the same relative expansion at a lower laser power, but the oscillations are also present. The oscillation period seems to be slightly lower than in the larger particles. Upon decreasing the excitation power (red curve in **Figure 2c**), the expansion is reduced to a maximum of 1.8%; the oscillations of the length are no more observable, and the LS state is already recovered after 100 ns. **Figure 2b** shows the curve of **Figure 2a** on a linear timescale. The vibration period tends to increase slightly with time. The length oscillations after saturation have a periodicity of somewhat less than 50 ns at a timescale 100 ns after the laser pulse. After some hundreds of ns, toward the ringdown of the vibration, the oscillation period increases to >100 ns. Another example, recorded on another particle and showing the reproducibility of the observations, is shown in **Figure S2** (Supporting Information).

The comparison with the experiments under 532 nm pulses (**Figure 1**) shows that the photoswitching time (≈ 80 ns to reach saturation), the vibration period (≈ 50 ns) and the decay time (≈ 1 μs) where the length variations disappear, are approximately the same for both wavelengths as soon as saturation is reached. The vibration periods and intensities seem to slightly differ from one particle to another and may be characteristic for each individual SCO particle. This can be explained by a different thermal contact to the substrate. Indeed, while 532 nm irradiation is directly absorbed by the particle, at 1064 nm the absorption by the carbon substrate and successive heat transfer to the particle might play a role. The contact between the substrate and the particle may add an additional barrier that slows down the photoswitching process. This could explain the steady increase observed after the 1064 nm pulse compared to 532 nm. Since the oscillations are mainly not coherent, in contrast to the ones observed in the picosecond timescale by optical or X-Ray studies, this might be another reason why the vibration periods slightly differ from one particle to another. It is due to the coupling between the elastic and thermal waves: the elastic waves are coherent, whereas the thermal waves are not. Moreover, we cannot exclude some damage due to the electron beam although the dose was reduced as much as possible, in particular during the search of a suitable particle with a continuous electron beam. The dose from the pulsed electron beam is comparatively low. TEM images of particles after prolonged electron or laser irradiation are shown

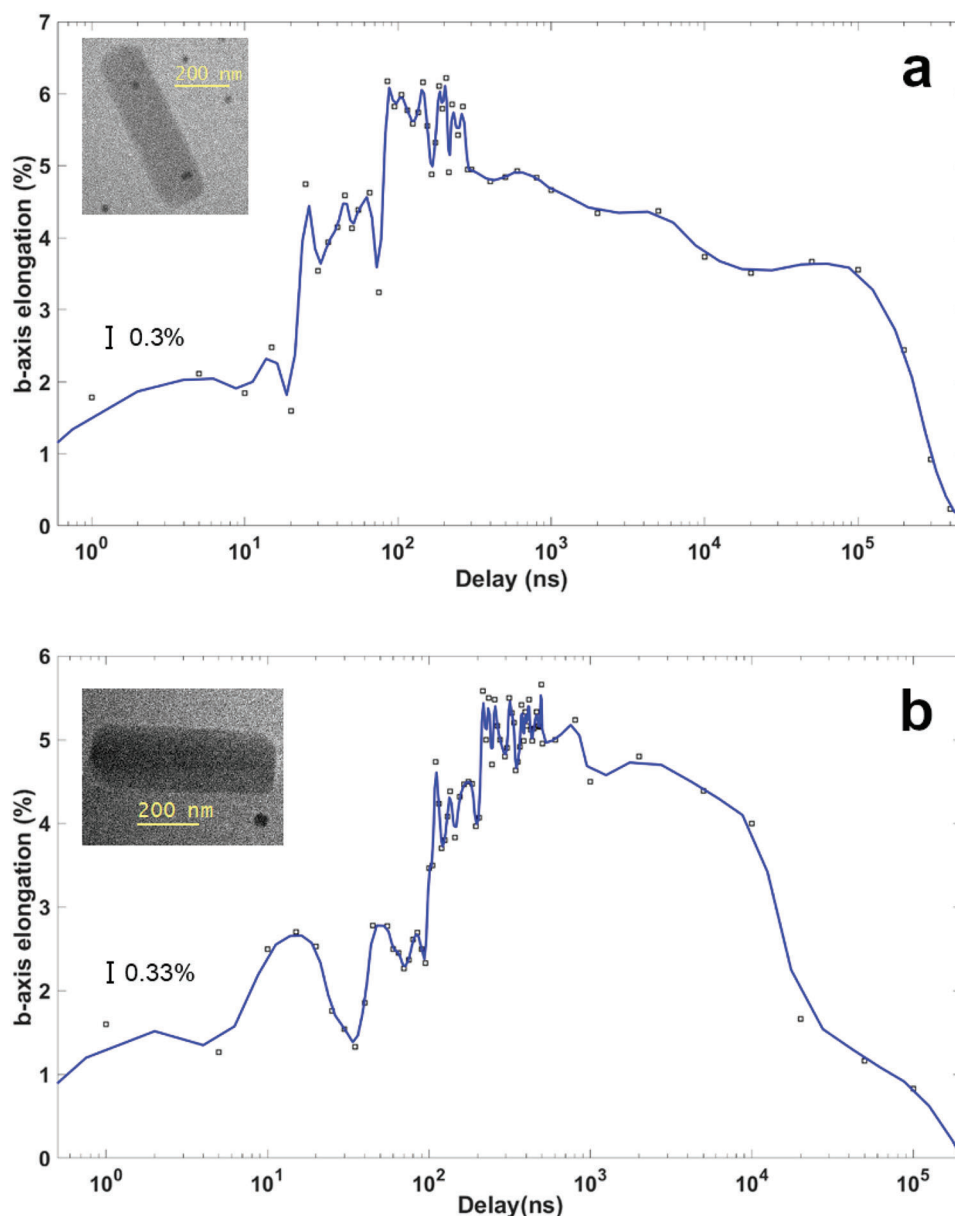


Figure 1. Time-resolved length measurements of two SCO particles with length of 600 nm. The excitation laser wavelength was 532 nm. a) Particle 1; the laser power on the specimen was $12 \mu\text{J cm}^{-2}$. b) Particle 2; the laser power on the specimen was $11 \mu\text{J cm}^{-2}$. TEM images of the respective particles are shown in the insets. The error bar of all measurements is shown on the left.

in Figures S4 and S5 (Supporting Information). These varying conditions could explain the variation from one particle to another.

A simple mechanical vibration in one state (LS or HS) cannot explain the oscillations because the observed vibration frequency is much lower than expected for a purely elastic vibration. The elastic modulus of $[\text{Fe}(\text{Htrz})_2\text{trz}](\text{BF}_4)$ is approximately $E = 20 \text{ GPa}$ and the density is $\rho = 1900 \text{ kg m}^{-3}$ in the low-spin and 1700 kg m^{-3} in the high spin state.^[30] The sound velocity in the material can be approximated by $c = (E/\rho)^{1/2}$, and with an average density of 1800 kg m^{-3} , we obtain $c = 3330 \text{ m s}^{-1}$. The elastic vibration period T of a rod of length l is $T = 2l/c$; so for a particle of $l = 600 \text{ nm}$, we would obtain a vibration period of $\approx 0.4 \text{ ns}$,

which is two orders of magnitude lower than the period of 50 ns that we have measured. Furthermore, the length changes during the vibration by $>1\%$ of the total length of the particles would be unusually high for the elastic vibration of a rigid crystal.

The observed vibration period of $\approx 50 \text{ ns}$ is close to the rise time from LS to HS after the laser pulses. It is obvious that a length vibration including the phase transition between LS and HS cannot be faster than the expansion time of a particle. By tentatively taking the above elasticity considerations, a vibration period of 50 ns should lead to a speed of the compression wave of only 24 m s^{-1} and an “effective elastic modulus” of the order 1 MPa. This is far from the experimental reality, even though the molecular lattice of SCO materials in the low-spin state is more rigid

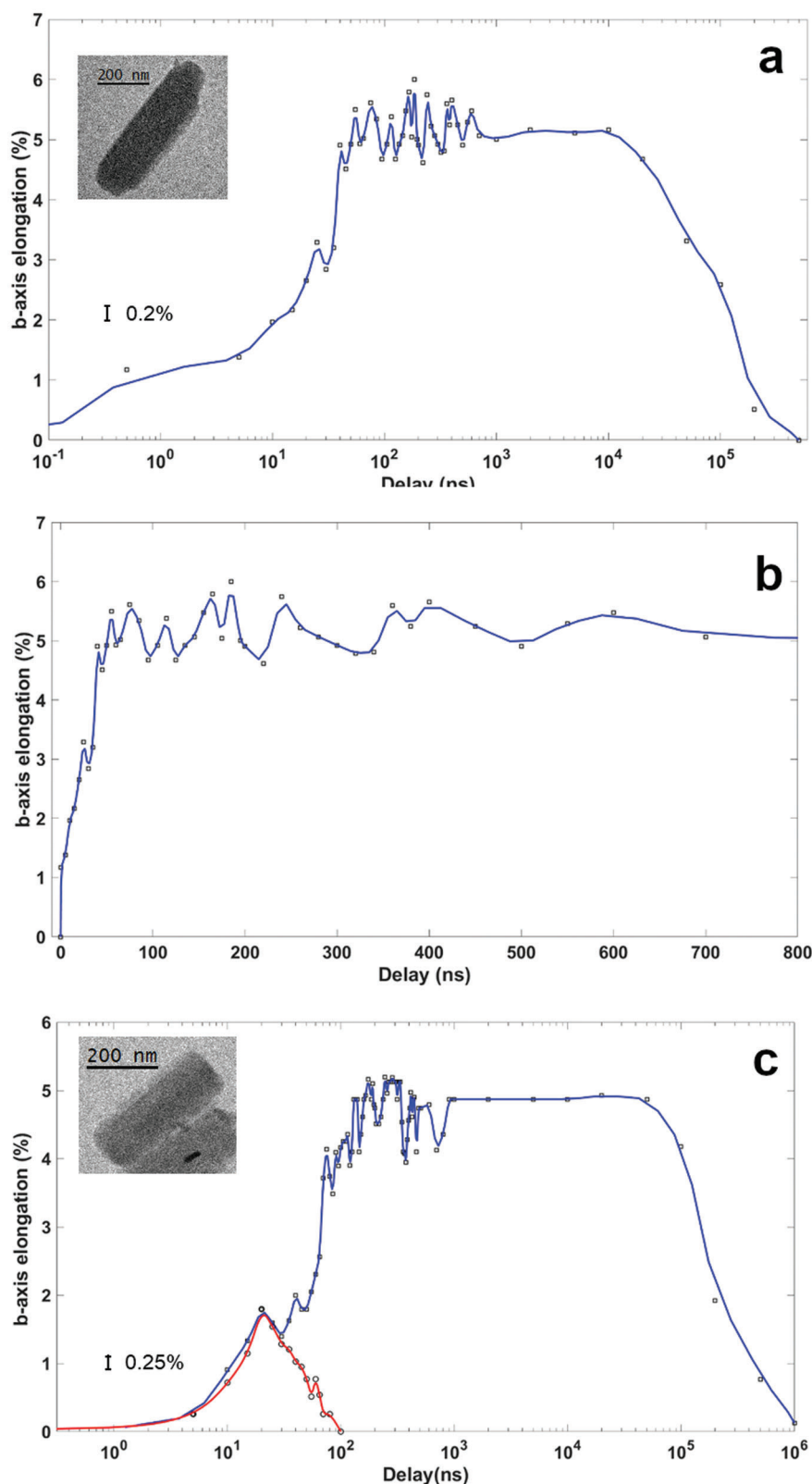


Figure 2. Time-resolved length measurements of two SCO particles at an excitation laser wavelength of 1064 nm. a,b) Particle length 600 nm; laser power 83 $\mu\text{J cm}^{-2}$; (a) shows the vibration on a logarithmic and b) on a linear time scale. c) Another particle with length 390 nm; laser power 64 $\mu\text{J cm}^{-2}$ (blue curve) and 26 $\mu\text{J cm}^{-2}$ (red curve).

than in the high spin state (differences in the elastic modulus of 30% have been reported).^[30,31] Therefore, we have to conclude that the length oscillations have to involve the repeated transformation between the two phases. They are due to a resonant vibration involving two competitive phase transformations (LS → HS and HS → LS) within one vibration period. This is an unusual behavior of a system undergoing a first order phase transformation where energy dissipation during the transformation normally prevents an oscillation between the two phases. Here, the elastic interaction between molecules of different spin states within an SCO crystal allows the system to vibrate between the two phases until energy dissipation leads to relaxation.

3. Discussion

In order to understand the observed behavior, numerical simulations were undertaken to evaluate the thermal and elastic effects on SCO particles. The system is described by a modified thermomechanical model^[32–34] that considers the molecules as rigid spheres in a 2D lattice, connected with springs.

In this model, the change of state of a molecule (LS to HS or HS to LS) is governed by a set of probabilities that involve local temperature and pressure together with intrinsic material parameters (Equation 1):

$$\begin{cases} P_{HS \rightarrow LS}^i = \frac{1}{\tau} \exp\left(\frac{D - k_B T \ln g}{2k_B T}\right) \exp\left(-\frac{E_a + \kappa p_i}{k_B T}\right) \\ P_{LS \rightarrow HS}^i = \frac{1}{\tau} \exp\left(-\frac{D - k_B T \ln g}{2k_B T}\right) \exp\left(-\frac{E_a - \kappa p_i}{k_B T}\right) \end{cases} \quad (1)$$

where τ is the normalization factor of the probabilities, D is the energy difference between the two states, T is the temperature of the system, $k_B \ln g$ is the entropy difference between the states, E_a is the activation energy of the HS state, p_i is the local pressure force acting on the i^{th} spin crossover site and κ is a constant that establishes how much the pressure influences the probabilities. The local stress on a particle i is the sum of the elastic forces that act on it. These probabilities are compared, in a typical Monte Carlo Arrhenius procedure, with a random number η between 0 and 1 to decide if a certain molecule should change state. One Monte Carlo step (MCS) is concluded when all the molecules have been tested once. If the switching probability to an opposite state is larger than η , the molecules are considered to undergo the transition.

When switching, a molecule changes its radius, and this change alters the elastic forces first on the immediate neighboring molecules and then, following the propagation of this perturbation, of all the other molecules in the system. Thus, after each MCS, the new position of each molecule is found by solving a system of ordinary differential equations (Equation 2):

$$\begin{cases} m \frac{d^2 x_i}{dt^2} = F_{x_i} - \mu \frac{dx_i}{dt} \\ m \frac{d^2 y_i}{dt^2} = F_{y_i} - \mu \frac{dy_i}{dt} \end{cases} \quad (2)$$

where x_i , y_i are the Cartesian coordinates of molecule i , μ is the damping constant, and F_{x_i} , F_{y_i} are the algebraic sums of forces acting on particle i in the two directions.

In order to account for the differences of elastic interaction along the 1D chain (coordination bonds) and between these

chains (weak hydrogen bonds), we have designed an elongated hexagonal lattice with intra-chain links depicted as springs of constant k_1 and unperturbed length L_1 and weaker and longer inter-chains links characterized by $k_2 = k_1/10$, $L_2 = 3L_1$ (Figure 3). Using the elementary cell represented in Figure 3 (inset), a rectangular system of 10620 molecules is built and used to simulate photoexcitation experiments.

At first, the system is in its LS equilibrium position with all the molecules having an initial temperature of 200 K. The photoexcitation taking place at $t = 0$ is simulated by instantaneously increasing the temperature of 75% of the molecules to 400 K, which is high enough to ensure a high value of the $P_{LS \rightarrow HS}$ switching probability for isolated molecules.

The sudden increase in radius of the excited molecules leads to internal stress and this translates into movement leading to new spatial positions for each molecule, positions that are found as solutions of the above-mentioned differential equation system. After finding the new positions, we compute the heat exchange between molecules and between the molecules and the environment (considered here as a thermal bath with a constant temperature of 200 K) considering the following differential equation (Equation 3):

$$\frac{dT_i}{dt} = -\alpha \cdot (T_i - \langle T_i^j \rangle) - \beta \cdot (T_i^{\text{edge}} - T_B) \quad (3)$$

where T_i is the temperature corresponding to the i^{th} molecule, $\langle T_i^j \rangle$ is the average temperature of all neighbors of the i^{th} molecule, α is the coefficient describing the heat exchange between molecules, T_B is the thermal bath temperature, T_i^{edge} is the temperature of molecules in contact with the thermal bath, and β is the heat transfer coefficient to the bath.

This complete one-simulation step consists of three stages:

- 1) one Monte Carlo step to decide which molecules switch,
- 2) one time step of solving the differential equation system to find the new positions, and
- 3) one heat exchange step among molecules.

After each step, different parameters are evaluated, for example, the physical parameter n_{HS} —the high spin fraction, as well as geometrical parameters describing the total length of the sample along different directions.

The results in Figure 3 show that after an initial increase in size in both directions, the length and width of the sample oscillate. Moreover, it evidences that the switching along the short axis occurs faster. The oscillations in the b-direction are in agreement with the experimental data, whereas the experimental measurements did not permit to observe the switching and the oscillations of the width of the particles due to the small absolute vibration amplitude and the limited image resolution in this experimental procedure.

We compared this switching-mediated oscillation (Figure 4a) with a purely elastic wave propagation through the sample (i.e., acoustic wave propagation, no switching is involved, Figure 4b). For this, we use the same model system with all the molecules in the same low spin state. After artificially producing an elastic deformation at one of the edges, we repeatedly solve the differential

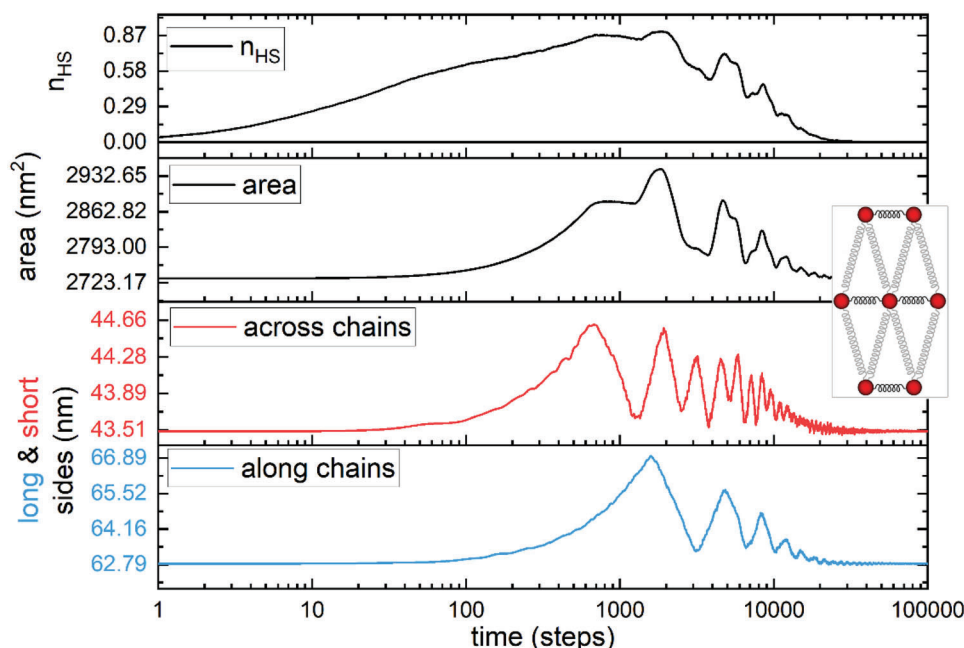


Figure 3. Time evolution of the fraction of molecules in the HS state n_{HS} and the geometry of the sample after photoexcitation. In the inset, a schematic representation of the elementary cell of the lattice used in simulations is shown. Black springs depict intra polymeric chains links while the grey springs depict the interactions between the chains.

equations system (stage (b)), neglecting the Monte Carlo step as well as the heat exchange steps (i.e., (a) and (c) stages).

In this model, the vibration of a SCO particle starts by “over-shooting” in the HS phase under a laser pulse. The excess of mechanical energy drives the lattice from expansion to compression where, under increasing pressure, the denser LS phase is favored. Repulsive forces and adiabatic temperature rise lead to the expansion and to the transition to HS again. It is therefore a resonant transition between the two phases of SCO. After a laser pulse, the particles are driven to a non-equilibrium state that is then fol-

lowed by an oscillatory relaxation into a temporarily stable state. At short timescales, an adiabatic behavior of the particles is expected where local heating favors the HS phase. It is therefore the elastic and thermal exchange between the molecules that determines the vibration period. Since only a fraction of the molecules within a crystal are normally excited by a laser pulse, the coupling between the molecules leads to the propagation of the transition until the whole crystal is saturated in one spin state.

The phase transformation between LS and HS is of first order, therefore, the dissipation of heat during the transition should

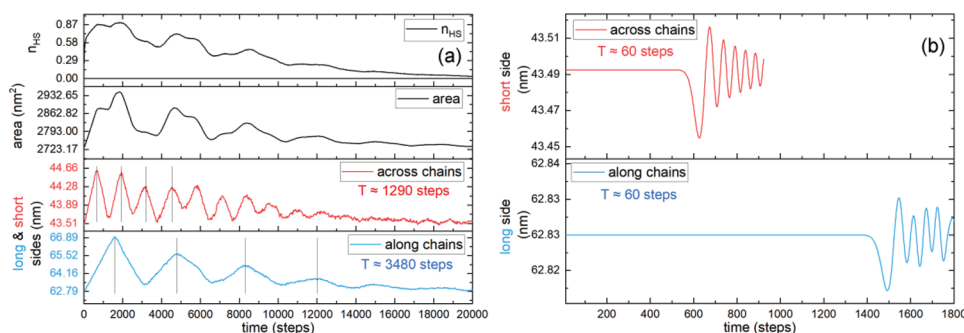


Figure 4. Switching-mediated oscillations (a) compared to purely acoustic oscillations without switching (b). The acoustic wave propagation leads to a much smaller oscillation period compared to the case when switching is also taken into account. In the switching-mediated oscillation of this simulation, a vibration period takes 410 time steps, whereas the simple elastic vibration period takes only 6 time steps. The ratio between these two vibration periods is 70 and can be compared to the estimates given above in the experimental section. The purely elastic vibration allows us to calibrate the time step in the simulation. The elastic vibration period of a 600 nm particle of 0.4 ns corresponds to 6 time steps, therefore the aforementioned factor of 70 leads to a vibration frequency of 35 ns in the simulations, which is close to the experimentally estimated value of 50 ns, corresponding to a vibration frequency of 20 MHz. The vibration frequency should be inversely proportional to the length of the particles. Since the lengths of the particles in this study (390 and 600 nm) are not very different and the vibration period can't be determined with sufficient accuracy, the length effect isn't clearly visible in Figure 2. The experimentally observed increase of the vibration period with time is not reproduced by the simulations. A nonlinear elastic behavior (i.e., where the elasticity modulus is higher at large elongation) could possibly explain the observations.

play an important role and lead to a damping of the vibration. Heat dissipation by thermal conductivity within the particles is slow. Conducting a temperature difference of 100 K through the SCO particles (600 nm) would take some μs ; therefore, a damping of the oscillation at the timescale of microseconds would be expected. This is in agreement with the observed vanishing of the vibration $\approx 1 \mu\text{s}$ after the laser pulse.

4. Conclusion

It is demonstrated that the laser-induced transformation from the LS to the HS state of a SCO crystal leads to considerable length vibrations during and after the expansion of the crystal. Due to the unique vibration characteristics of each individual SCO particle, this oscillation is not visible in macroscopic measurements, for example, by X-ray diffraction or magnetic measurements, where an average over many SCO particles is taken. By time-resolved TEM, where individual particles are analyzed, the oscillatory effect becomes finally visible. These transient oscillations are slightly dependent on the size of the particle and the irradiation wavelength and cannot be explained by a pure propagation of a simple acoustic wave, which does not involve switching of the molecules and should propagate much faster. The oscillation between the two phases of SCO can be considered as a transient resonant phase transformation that is due to the coupling between the elastic and thermal waves within the crystal and the intermolecular interaction during the phase transformation. The same behavior should also be observable in other SCO materials (and in breathing materials in general) where the molecules interact by the exchange of elastic forces. The present experiments are complementary to previous studies in the femto- or picosecond range. Since phase transformations of first order are generally irreversible if the outer conditions (pressure, temperature, etc.) do not change, SCO materials are a unique system where such a resonant oscillation between two phases can be studied. In other materials passing through first order phase transformations, such a behavior does not occur because the interaction between neighboring atoms or molecules is purely elastic and propagates with the speed of sound.

The observed oscillations of SCO particles have to be considered in applications as photoswitches. Due to the oscillations, the state of the particles (LS or HS) may not be well defined during the switching process and up to some microseconds after the switching. In optoelectronic or mechanical devices, this may have an impact on the time scale needed to reach an equilibrium in the excited state. This may lead to fatigue at the interface between SCO particles and electrodes or surfaces in devices. For laser powers below the saturation (maximum expansion) of the SCO particles (Figure 2), the oscillations could possibly be avoided.

5. Experimental Section

The synthesis of $[\text{Fe}(\text{Htrz})_2\text{trz}](\text{BF}_4)$ particles was performed following the procedure described in a previous report^[35] by mixing 1.2 M of $\text{Fe}(\text{BF}_4)_2 \cdot 6\text{H}_2\text{O}$ salt to three equivalents of 1H-1,2,4-triazole (Htrz), both dissolved in a 60%:40% water:ethanol mixture. The particles were isolated by centrifugation and dried overnight in ambient conditions. The SCO particles were dispersed in ethanol and deposited either on multilayer

graphene sheets or amorphous carbon films that were held by standard copper grids for electron microscopy studies (a TEM image with some SCO particles is shown in Figure S1, Supporting Information).

Time-resolved length measurements of individual SCO nanoparticles were undertaken by ultrafast transmission electron microscopy.^[28,36–38] In the present setup, two electronically synchronized nanosecond lasers, both emitting 7 ns pulses, were used. In a pump-probe approach, the particles on the TEM grid were exposed to pulses from one laser whereas the pulses from the other laser were transformed to the 5th harmonic (213 nm) and focused onto the disk-shaped tantalum photocathode of the TEM where photoelectron bunches are created. By electronically adjusting the delay between the two lasers, time-resolved information about the specimen was obtained with nanometer resolution. Pump laser pulses with wavelengths between 532 and 1064 nm were chosen to study the influence of the absorption of SCO at different wavelengths. The absorption of $[\text{Fe}(\text{Htrz})_2\text{trz}](\text{BF}_4)$ at 532 nm is ≈ 5 times higher than at 1064 nm.^[39] Since the length changes of the SCO particles under laser pulses were reversible, the experiments were carried out in a stroboscopic approach with a repetition frequency of 20 Hz. The total exposure times of the images were typically 60 s so that 1200 pump-probe cycles were acquired for each length measurement. The time resolution of this setup corresponded approximately to the laser pulse duration of 7 ns. The experiments were carried out with different energies of the pump laser pulses in the range from a few μJ to some tens of nJ per pulse on the specimen (corresponding to few or tens of $\mu\text{J cm}^{-2}$, given the laser spot of $\approx 4 \times 10^4 \mu\text{m}^2$ on the sample).

A contrast profile in the images of the SCO particles with lengths between 300 and 600 nm and width of 200 nm (the width in two perpendicular orientations was the same) was used to measure the length along the b-axis, which was the axis of maximum expansion.^[28] After averaging along the edge of the particle, a precision of the length measurement of $\approx 0.2 \text{ nm}$ was achieved, which was mainly limited by noise in the images. Measurements by electron diffraction turned out to be difficult at the low coherence of the electron beam, and the results would not be conclusive due to different lattice spacings throughout the crystals during their expansion or contraction (see below).

To exclude the influence of possible vibrations of the specimen support or other sources of error, a time-resolved length measurement of deactivated SCO particles under laser pulses was undertaken. The deactivation was achieved by extended electron irradiation in the TEM until radiation damage prevented any length changes of SCO under laser pulses. No considerable length changes and in particular no length oscillations were observable in such deactivated particles (see Figures S3 and S4, Supporting Information).

Supporting Information

Supporting Information is available from the Wiley Online Library or from the author.

Acknowledgements

Funding by the Agence Nationale de Recherche (contract ANR-22-CE09-0033-01) and the network METSA (Réseau national de plateformes en microscopie électronique en transmission et sonde atomique) was gratefully acknowledged. The work of C. E. was supported by a grant of the Romanian Ministry of Research, Innovation and Digitisation, CNCS/CCDI-UEFISCDI, Project No. PN-III-P4-ID-PCE-2020-1946, within PNCDIII.

Conflict of Interest

The authors declare no conflict of interest.

Data Availability Statement

The data that support the findings of this study are available from the corresponding author upon reasonable request.

Keywords

Monte Carlo calculations, phase transformations, spin crossover materials, ultrafast transmission electron microscopy

Received: May 10, 2023
Published online:

- [1] S. Nemat-Nasser, S. Nemat-Nasser, T. Plaisted, A. Starr, A. Vakil Amirkhizi, in *Biomimetics: biologically inspired technologies*, CRC Press, Boca Raton, FL **2005**.
- [2] N. Konstantinov, A. Tauzin, U. Noumbe, D. Dragoe, B. Kundys, H. Majjad, A. Brosseau, M. Lenertz, A. Singh, S. Berciaud, M.-L. Boillot, B. Doudin, T. Mallah, J.-F. Dayen, *J. Mater. Chem. C* **2021**, 9, 2712.
- [3] J.-F. Dayen, N. Konstantinov, M. Palluel, N. Daro, M. Soliman, G. Chastanet, B. Doudin, *Mater. Horiz.* **2021**, 8, 2310.
- [4] M. D. Manrique-Juarez, S. Rat, L. Salmon, G. Molnar, C. M. Quintero, L. Nicu, H. J. Shepherd, A. Bousseksou, *Coord. Chem. Rev.* **2016**, 308, 395.
- [5] J. Dugay, M. Gimenez-Marquès, W. J. Venstra, R. Torres-Cavanillas, U. N. Sheambarsing, N. Manca, E. Coronado, H. S. J. van der Zant, *J. Phys. Chem. C* **2019**, 123, 6778.
- [6] H. J. Shepherd, I. A. Gural'skiy, C. M. Quintero, S. Tricard, L. Salmon, G. Molnar, A. Bousseksou, *Nature. Comm.* **2013**, 4, 3607.
- [7] T. Miyamachi, M. Gruber, V. Davesne, M. Bowen, S. Boukari, L. Joly, F. Scheurer, G. Rogez, T. K. Yamada, P. Ohresser, E. Beaupaire, W. Wulffke, *Nature. Comm.* **2012**, 3, 938.
- [8] M. Urdampilleta, C. Ayela, P.-H. Ducrot, D. Rosario-Amorin, A. Mondal, M. Rouzières, P. Dechambenoit, C. Mathonière, F. Mathieu, I. Dufour, R. Clérac, *Sci. Rep.* **2018**, 8, 8016.
- [9] M. D. Manrique-Juarez, S. Rat, F. Mathieu, D. Saya, I. Séguy, T. Leïchle, L. Nicu, L. Salmon, G. Molnar, A. Bousseksou, *Appl. Phys. Lett.* **2016**, 109, 061903.
- [10] F. Prins, M. Monrabal-Capilla, E. A. Osorio, E. Coronado, H. S. J. van der Zant, *Adv. Mater.* **2011**, 23, 1545.
- [11] K. Senthil Kumar, M. Ruben, *Angew Chem Int Ed Engl* **2021**, 60, 7502.
- [12] C. Lefter, R. Tan, S. Tricard, J. Dugay, G. Molnar, L. Salmon, J. Carrey, A. Rotaru, A. Bousseksou, *Polyhedron* **2015**, 102, 434.
- [13] E. Resines-Urien, E. Fernandez-Bartolome, A. Martinez-Martinez, A. Gamonal, L. Piñeiro-López, J. S. Costa, *Chem. Soc. Rev.* **2023**, 52, 705.
- [14] A. Lapresta-Fernandez, S. Titos-Padilla, J. Manuel Herrera, A. Salinas-Castillo, E. Colacio, L. Fermin Capitan Vallvey, *Chem. Commun.* **2013**, 49, 288.
- [15] K. Boukheddaden, M. H. Ritti, G. Bouchez, M. Sy, M. M. Dîrtu, M. Parlier, J. Linares, Y. Garcia, *J. Phys. Chem. C* **2018**, 122, 7597.
- [16] P. Gülich, H. A. Goodwin, *Spin crossover - an overall perspective, Spin Crossover in Transition Metal Compounds I*, **2004**, pp. 1–47.
- [17] P. G. Guionneau, M. Marchivie, G. Chastanet, *Chem. - Eur. J.* **2021**, 27, 1483.
- [18] C. Enachescu, W. Nicolazzi, *C. R. Chimie* **2018**, 21, 1179.
- [19] L. Salmon, L. Catala, *C. R. Chimie* **2018**, 21, 1230.
- [20] M. Chergui, E. Collet, *Chem. Rev.* **2017**, 117, 11025.
- [21] R. Bertoni, M. Lorenc, A. Tissot, M. L. Boillot, E. Collet, *Coord. Chem. Rev.* **2015**, 282, 66.
- [22] R. Bertoni, M. Lorenc, H. Cailleau, A. Tissot, J. Laisney, M. L. Boillot, L. Stoleriu, A. Stancu, C. Enachescu, E. Collet, *Nat. Mater.* **2016**, 15, 606.
- [23] R. Bertoni, M. Cammarata, M. Lorenc, S. F. Matar, J. F. Letard, H. T. Lemke, E. Collet, *Acc. Chem. Res.* **2015**, 48, 774.
- [24] G. Chastanet, M. Lorenc, R. Bertoni, C. Desplanches, *C. R. Chimie* **2018**, 21, 1075.
- [25] S. Zerdane, M. Hervé, S. Mazerat, L. Catala, R. Alonso-Mori, J. M. Glowina, S. Song, M. Levantino, T. Mallah, M. Cammarata, E. Collet, *Faraday Discuss.* **2022**, 237, 224.
- [26] R. M. Van der Veen, O.-H. Kwon, A. Tissot, A. Hauser, A. H. Zewail, *Nature. Chem.* **2013**, 5, 395.
- [27] S. T. Park, R. M. van der Veen, *Struct. Dyn.* **2017**, 4, 044028.
- [28] Y. Hu, M. Picher, N. M. Tran, M. Palluel, L. Stoleriu, N. Daro, S. Mornet, C. Enachescu, E. Freysz, F. Banhart, G. Chastanet, *Adv. Materials* **2021**, 33, 2105586.
- [29] A. Grosjean, P. Négrier, P. Bordet, C. Etrillard, D. Mondieg, S. Pechev, E. Lebraud, J.-F. Létard, P. Guionneau, *Eur. J. Inorg. Chem.* **2013**, 5-6, 796.
- [30] D. Paliwoda, L. Vendier, L. Getzner, F. Alabarse, D. Comboni, B. Martin, S. E. Alavi, M. Piedrahita Bello, L. Salmon, W. Nicolazzi, G. Molnar, A. Bousseksou, *Cryst. Growth Design* **2023**, 23, 1903.
- [31] M. Mikolasek, M. D. Manrique-Juarez, H. J. Shepherd, K. Ridier, S. Rat, V. Shalabaeva, A.-C. Bas, I. E. Collings, F. Mathieu, J. Cacheux, T. Leichle, L. Nicu, W. Nicolazzi, L. Salmon, G. Molnár, A. Bousseksou, *J. Am. Chem. Soc.* **2018**, 140, 8970.
- [32] C. Enachescu, L. Stoleriu, M. Nishino, S. Miyashita, A. Stancu, M. Lorenc, R. Bertoni, H. Cailleau, E. Collet, *Phys. Rev. B* **2017**, 95, 224107.
- [33] A. I. Popa, L. Stoleriu, C. Enachescu, *J. Appl. Phys.* **2021**, 129, 131101.
- [34] A. Railean, M. Kelai, A. Bellec, V. Repain, M.vL. Boillot, T. Mallah, L. Stoleriu, C. Enachescu, *Phys. Rev. B* **2023**, 107, 014304.
- [35] M. Palluel, L. El Khoury, N. Daro, S. Buffière, M. Josse, M. Marchivie, G. Chastanet, *Inorg. Chem. Front.* **2021**, 8, 3697.
- [36] K. Bückner, M. Picher, O. Crégut, T. LaGrange, B. W. Reed, S. T. Park, D. J. Masiel, F. Banhart, *Ultramicroscopy* **2016**, 171, 8.
- [37] M. Picher, K. Bückner, T. LaGrange, F. Banhart, *Ultramicroscopy* **2018**, 188, 41.
- [38] S. K. Sinha, A. Khammari, M. Picher, F. Roulland, N. Viart, T. LaGrange, F. Banhart, *Nat. Commun.* **2019**, 10, 3648.
- [39] M. Palluel, N. M. Tran, N. Daro, S. Buffière, S. Mornet, E. Freysz, G. Chastanet, *Adv. Funct. Materials* **2020**, 30, 2000447.